In Vitro Cellular & Developmental Biology - Animal (2024) 60:54–66
https://doi.org/10.1007/s11626-023-00834-7

Cucumber seed polypeptides regulate RANKL-induced osteoclastogenesis through OPG/RANKL/RANK and NF-κB

Tao Yu[1] · Xiao Liu[2] · Meng Jiang[2] · Yuanyue Li[1] · Heng Su[3] · Ben Niu[3]

Received: 3 September 2023 / Accepted: 29 November 2023 / Published online: 20 December 2023 / Editor: Tetsuji Okamoto

Abstract
Postmenopausal osteoporosis (PMOP) is a common disease that endangers the health of elderly women. Cucumber seeds have shown excellent therapeutic effects on PMOP, but the mechanism of cucumber seed peptide (CSP) remains unclear. The expression levels of NF-κB and osteoclast-related genes were detected by RT-qPCR. The levels of apoptosis-related proteins were detected by Western blotting. Nuclear translocation of NF-κB p65 and osteoclast formation were detected by immunofluorescence and tartrate-resistant acid phosphatase (TRAP) staining, respectively. ELISA was used to detect the expression levels of OPG, M-CSF, and RANKL. Hematoxylin–eosin (H&E) and TRAP staining were used to observe the effects of CSP on bone formation. In RAW264.7 cells, CSP (0.4 mg/L, 4 mg/L, and 40 mg/L) effectively inhibited the expression of osteoclast-related genes (Cathepsin-K, MT1-MMP, MMP-9, and TRAP). TRAP-positive multinucleated giant cells gradually decreased. Furthermore, NF-κB pathway activation downstream of RANK was inhibited. In bone marrow stromal cells (BMSCs), the expression levels of M-CSF and RANKL gradually decreased, and OPG gradually increased with increasing CSP concentrations. Treatment of RAW264.7 cells with pyrrolidine dithiocarbamate (PDTC, an inhibitor of NF-κB) prevented the formation of osteoclasts. Treatment with different concentrations of CSP effectively decreased the levels of RANKL and M-CSF in rat serum and increased the expression of OPG in the oophorectomy (OVX) rat model. Furthermore, different concentrations of CSP could ameliorate the loss of bone structure and inhibit the formation of osteoclasts in rats. CSP inhibits osteoclastogenesis by regulating the OPG/RANKL/RANK pathway and inhibiting the NF-kB pathway.

Keywords Postmenopausal osteoporosis · Cucumber seed peptide · OPG/RANKL/RANK pathways · NF-κB pathways

Introduction

Postmenopausal osteoporosis (PMOP) is the most common type of osteoporosis caused by estrogen deficiency and typically occurs in postmenopausal women (Feng *et al*. 2021). Postmenopausal osteoporosis is mainly treated with bisphosphonates, hormone replacement therapy (HRT), and selective estrogen receptor modulators (SERMs), all of which are based on therapies that target the activity of bone-resorbing osteoclasts (Arceo-Mendoza and Camacho 2021; Brown 2021). However, these drugs can only reduce the sensitivity to fractures by approximately 50% (McNamara 2010). Therefore, new drugs without adverse side effects are needed for the treatment of osteoporosis.

Normal bone metabolism is managed bone destruction and bone formation, which maintain a dynamic balance. The osteoprotegerin (OPG)/receptor activator of nuclear factor NF-κB ligand (RANKL)/receptor activator of NF-κB (RANK) system is a signaling pathway that functions during bone reconstruction and osteoclast differentiation (Kovács *et al*. 2019). OPG is secreted by osteoblasts and is a RANKL bait receptor, which, as the only negative regulator of osteoclasts, can prevent the binding of osteoclasts to RANKL and block signal transduction, thus preventing bone resorption (Udagawa *et al*. 2021) (Lloyd *et al*. 2008). Studies

✉ Ben Niu
niubenynsdyrmyy@163.com

[1] Department of Gynecology, The First People's Hospital of Yunnan Province, The Affiliated Hospital of Kunming University of Science and Technology, Kunming 650032, Yunnan, China

[2] Yunnan University of Traditional Chinese Medicine, Kunming 650500, Yunnan, China

[3] Department of Endocrinology and Metabolism, The First People's Hospital of Yunnan Province, The Affiliated Hospital of Kunming University of Science and Technology, No. 157 Jinbi Road, KunmingYunnan 650032, China

have shown that after OPG knockdown, mice exhibit severe osteoporosis. RANKL belongs to the tumor necrosis factor ligand superfamily and is the only factor known to date that promotes the differentiation of osteoclast precursor cells into osteoclasts and enhances the activity of mature osteoclasts (McDonald *et al*. 2021). RANK is the only known receptor of RANKL, which is highly expressed on the surface of osteoclastic precursor cells and mature osteoclasts, directly promotes the differentiation and activation, and prevents osteoclast apoptosis. The binding of RANKL and RANK is critical for osteoclast survival, differentiation, and activation (Yasuda 2021). Therefore, the OPG/RANKL/RANK system is critical in bone remodeling and osteoclast differentiation.

The binding of RANKL produced by osteoblasts to RANK on osteoclasts can promote osteoclast differentiation and maturation (Dong *et al*. 2022). Certain drugs have been shown to alleviate PMOP through the NF-κB, AKT, and OPG/RANKL/RANK pathways. For example, fructose 1,6-diphosphate strontium and salmon calcitonin plus aspirin prevent bone loss in postmenopausal osteoporotic rats by regulating the OPG/RANKL/RANK pathway (Ma *et al*. 2012; Wei *et al*. 2015). Moreover, β-amyloid peptides promote bone formation by regulating OPG/RANKL/RANK and Wnt/β-catenin signaling (Yang *et al*. 2020). Dimethylbisphosphonate plus 99Tc-MDP can induce apoptosis in RAW264.7 cells by regulating the OPG/RANKL/RANK pathway, inhibiting RANK protein expression, and promoting MC3T3-E1 cell proliferation (Shen *et al*. 2019). Chen *et al*. (2020) reported that shikonin prevented osteoclastogenesis by inhibiting the downstream NF-κB signaling pathway via TRAF6 and RANK in osteoclasts in vitro. These findings have led to new ideas for the development and application of osteoporosis treatments.

Most researchers acknowledge the importance of nutrients in plant seeds for human health, and so the beneficial effects of various seeds, such as Anudeep seeds, on the host immune system have been examined (Anudeep *et al*. 2016). Cucumber seeds have a long history of providing remarkable results in folk treatments of diseases such as osteoporosis, osteoarthritis, and cervical spondylosis and have shown excellent therapeutic effects (Lin *et al*. 2019). Numerous studies have shown that peptides possess antioxidant, antihypertensive, antithrombotic, hypolipidemic, ACE inhibitory, immunoregulatory, and mineral absorption- or bioavailability-enhancing activities (Mohan *et al*. 2016). One study reported that casein phosphopeptides (CPPs) could promote the absorption of minerals in organisms (Rajapakse *et al*. 2005). Lin *et al*. (2019) showed that RANKL/M-CSF-induced osteoclast differentiation could be inhibited by deer cucurbit polypeptide (CCP) and simultaneously inhibit the activation of mid-downstream osteoclast-specific genes and transcription factors in RAW264.7 cells. Liquid fermentation of cucumber seeds by *Bacillus subtilis* showed that a specific cucumber seed peptide (CSP) was successfully produced (Wang *et al*. 2017). However, the mechanism of CSP in the host has not been reported.

However, whether the peptides (CSP) in cucumber seed powder can regulate postmenopausal osteoporosis through the OPG/RANK/RANKL and NF-KB pathways remains unclear. Consequently, we will continue to study the molecular and regulatory mechanisms of cucumber powder polypeptide in the prevention of postmenopausal osteoporosis.

Materials and methods

Osteoclast culture RAW264.7 cells and BMSCs from the ATCC (Rockefeller, Maryland) cell bank were seeded in 10% fetal bovine serum and high glucose medium, placed at 37℃, and cultured under 5% CO_2. During this time, the medium was changed every 2 d, and the cells were subcultured after 3–4 d. To induce osteoclast differentiation, cells within 15 passages were collected and seeded at a density of 2×10^4 cells in 1 mL of medium. After the cells adhered to the plate for 24 h under the abovementioned culture conditions, the induction and differentiation medium was

Table 1. Primer sequences

Name	Primer sequence
Cathepsin-K	Forward: 5′-CTTCCAATACGTGCAGCAGA-3′
	Reverse: 5′-TCTTCAGGGCTTTCTCGTTC-3′
TRAP	Forward: 5′- GCTGGAAACCATGATCACCT-3′
	Reverse: 5′- GAGTTGCCACACAGCATCAC-3′
MT1-MMP	Forward: 5′-CCCCGCTGCGGTGTTCCAGAC-3′
	Reverse: 5′-CTCCGCGGAGTCAAAGTGGGT-3′
MMP-9	Forward: 5′-CGTCGTGATCCCCACTTACT-3′
	Reverse: 5′-AACACACAGGGTTTGCCTTC-3′
M-CSF	Forward: 5′-GAACAGCCTGTCCCATCCATC-3′
	Reverse: 5′-TGAGGCCAGCTCAGTGCAA-3′
RANKL	Forward: 5′-CAGCATCGCTCTGTTCCTGTA-3′
	Reverse: 5′-CTGCGTTTTCATGGAGTCTCA-3′
OPG	Forward: 5′-ACCCAGAAACTGGTCATCAGC-3′
	Reverse: 5′-CTGCAATACACACACTCATCACT-3′
RANK	Forward: 5′-GGACGGTGTTGCAGCAGAT-3′
	Reverse: 5′-GCAGTCTGAGTTCCAGTGGTA-3′
NFATc1	Forward: 5′-TGGAGAAGCAGAGCACAGAC-3′
	Reverse: 5′-GCGGAAAGGTGGTATCTCAA-3′
c-Fos	Forward: 5′-CAAGCGGAGACAGATCAACTTG-3′
	Reverse: 5′-TTTCCTTCTCTTTCAGCAGATTGG-3′
GAPDH	Forward: 5′-AACTTTGGCATTGTGGAAGG-3′
	Reverse: 5′-ACACATTGGGGGTAGGAACA-3′

changed (basal medium + 50 ng/mL RANKL), and the cells were cultured for 6 d. CSP was obtained from Beyotime Science and Technology Co., Ltd. (Shanghai, China) and contained a mixture of several peptides (the molecular weights were approximately 3 ~ 12 kDa). Different concentrations of CSP (0.4 mg/L, 4 mg/L, and 40 mg/L) were cultured with RANKL-treated RAW264.7 cells or BMSCs.

Reverse transcription-quantitative polymerase chain reaction (RT-qPCR) We extracted total RNA from tissues and cells using a Total RNA Extractor Kit (Sangon Biotech, Shanghai, China). A cDNA synthesis kit (Vazyme, Nanjing, China) was used to reverse transcribe 2 μg of mRNA into cDNA, which was then diluted 10 times. One microliter of the prepared cDNA was used for qPCR. All primers (Table 1) used in this study were designed with Premier 5.0. The confidence of the PCR results was assessed based on the dissociation curve and cycle threshold (CT) values. The results were calculated by the $2^{-\Delta\Delta Ct}$ method after at least 3 repetitions. GAPDH was used to quantify the expression of various genes.

Western blot analysis In this study, proteins were extracted using a protein extraction kit (Sangon Biotech), and the bicinchoninic acid (BCA) assay (Sangon Biotech) was used to determine the total protein content. After denaturation for 5 min, total proteins were separated by 10% SDS-PAGE and transferred to polyvinylidene fluoride (PVDF) membranes (Millipore, Burlington, MA) via a constant current flow at 200 mA. Subsequently, the PVDF membranes were incubated with Bcl-2 (1:10,000), Bax (1:2000), Caspase-3 (1:5000), M-CSF (1:1000), RANKL (1:3000), OPG (1:3000), p-p65 (1:1000), p65 (1:1000), p-p38 (1:1000), p38 (1:5000), p-JNK (1:1000), JNK (1:1000), p-AKT (1:2000), AKT (1:2000), p-ERK (1:1000), ERK (1:1000), RANK (1:2000), NF-κB (1:1000), NFATc1 (1:10,000), and c-Fos (1:1000) antibodies (Abcam, Cambridge, MA) for 12 h at 4°C. TBS buffer was used to wash the PVDF membranes,

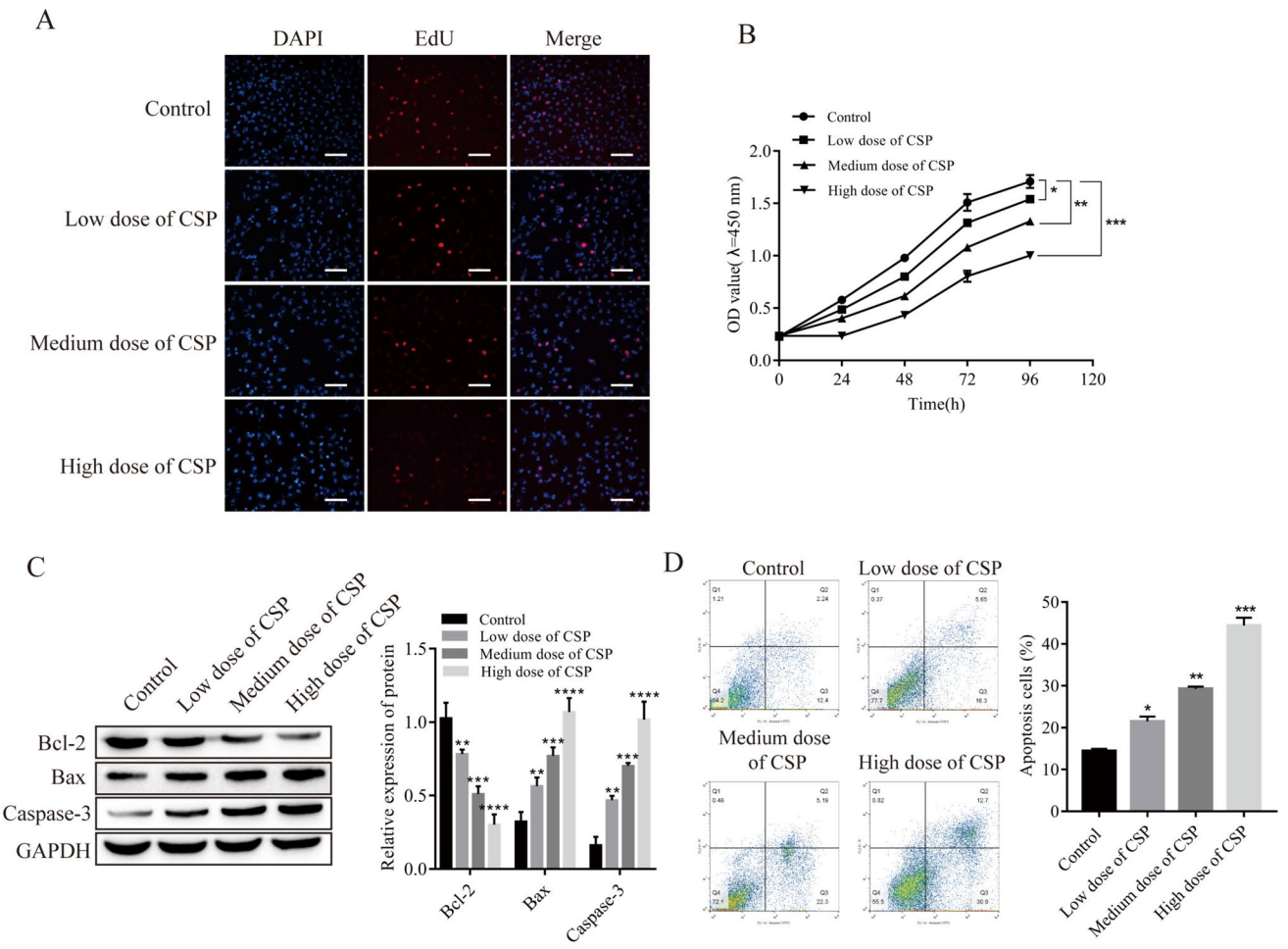

Figure 1. Effects of CSP on apoptosis in RAW264.7 cells ($n = 3$). (*A*) Cell proliferation was detected by EdU assays (*scale bar* = 100 μm). (*B*) Cell proliferation was detected by CCK-8 assays. (*C*) The expression of apoptosis-related proteins was detected by Western blot analysis. (*D*) Apoptosis was detected by flow cytometry. $^{*}P < 0.5$, $^{**}P < 0.01$, $^{***}P < 0.001$, $^{****}P < 0.0001$ vs. control. Cells were incubated with CSP for 48 h. Low, medium, and high doses of CPS refer to 0.4 mg/L, 4 mg/L, and 40 mg/L CPS, respectively.

and secondary antibodies (Abcam) were added and incubated at room temperature for 1 h. After the membranes were washed three times, chemiluminescent reagents were added, and the grayscale values of the bands were analyzed using ImageJ software. Each experiment was independently repeated 3 times. GAPDH was used to quantify the expression of various proteins.

CCK-8 assay We added 100 μL of the cell suspension (4×10^4 cells/mL) to a 96-well plate, which was then placed in a 5% CO_2 incubator at 37°C for 24 h. After the cells were transfected or treated, ten microliters of CCK-8 reagent was added and incubated for 2 h. Finally, an enzyme reader (ELX800, BioTeK, Winooski, VT) was used to measure the absorbance at 450 nm. Each experiment was independently repeated 3 times.

5-Ethynyl-2′-deoxyuridine (EdU) assay The EdU reagent was diluted according to the instructions of the EdU kit (RIBOBIO, Guangzhou, China), after which 100 μL of 50 μM EdU reagent was added to the cells and incubated for 2 h. After the solution was discarded, the cells were washed with phosphate-buffered saline (PBS) and fixed with 4% paraformaldehyde solution for 30 min. After the paraformaldehyde solution was discarded, the cells were incubated with 2 mg/mL glycine solution on a decolorizing shaker for 5 min,

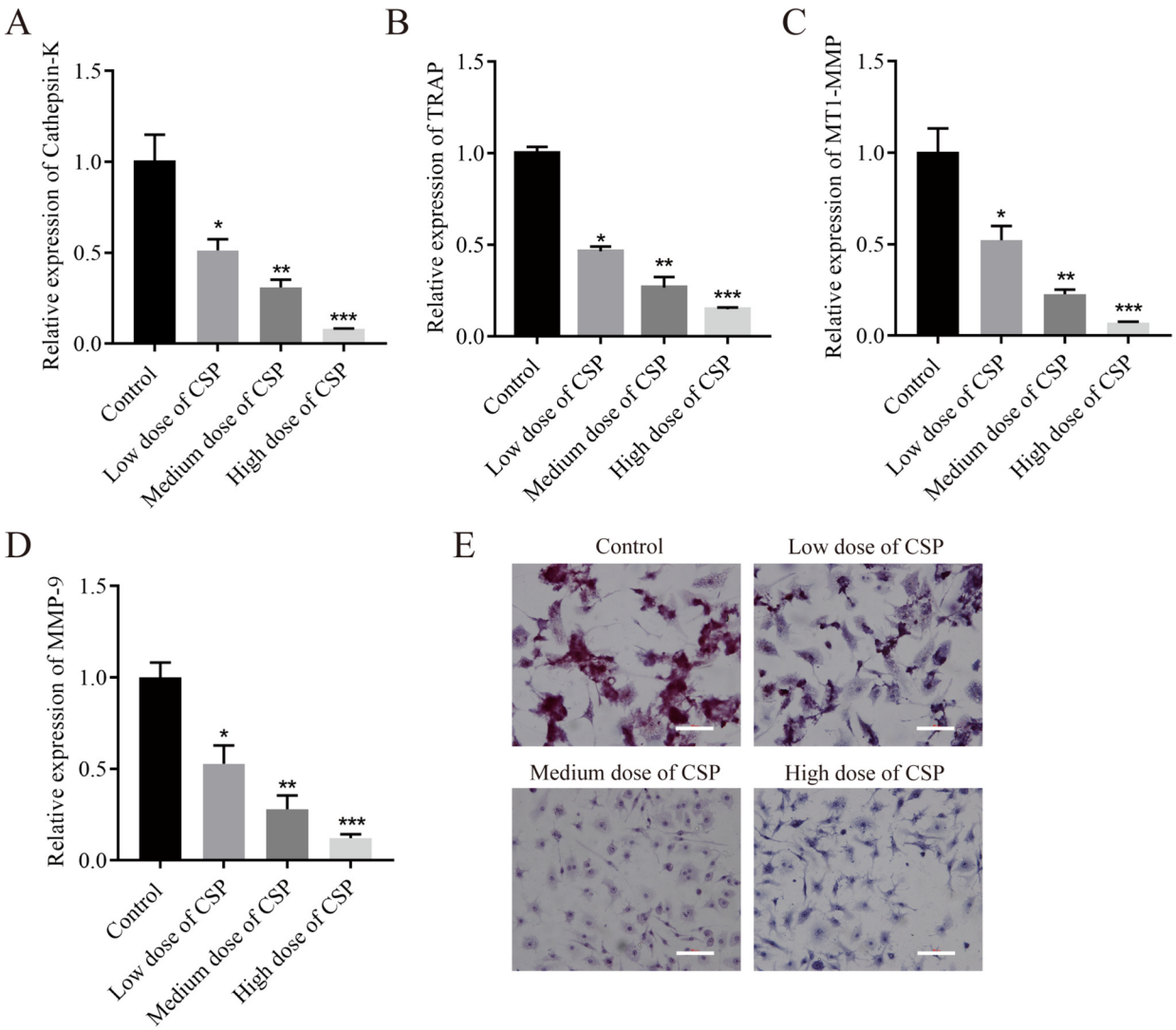

Figure 2. CSP inhibits osteoclast formation in a dose-dependent manner in RAW264.7 cells ($n=3$). (*A–D*) The expression levels of Cathepsin-K, TRAP, MT1-MMP, and MMP-9 were detected by RT-qPCR. (*E*) TRAP staining was performed to determine the number of positive multinucleated giant cells (*scale bar* = 100 μm). $^*P<0.5$, $^{**}P<0.01$, $^{***}P<0.001$ vs. control. Cells were incubated with CSP for 48 h. Low, medium, and high doses of CPS refer to 0.4 mg/L, 4 mg/L, and 40 mg/L CPS, respectively.

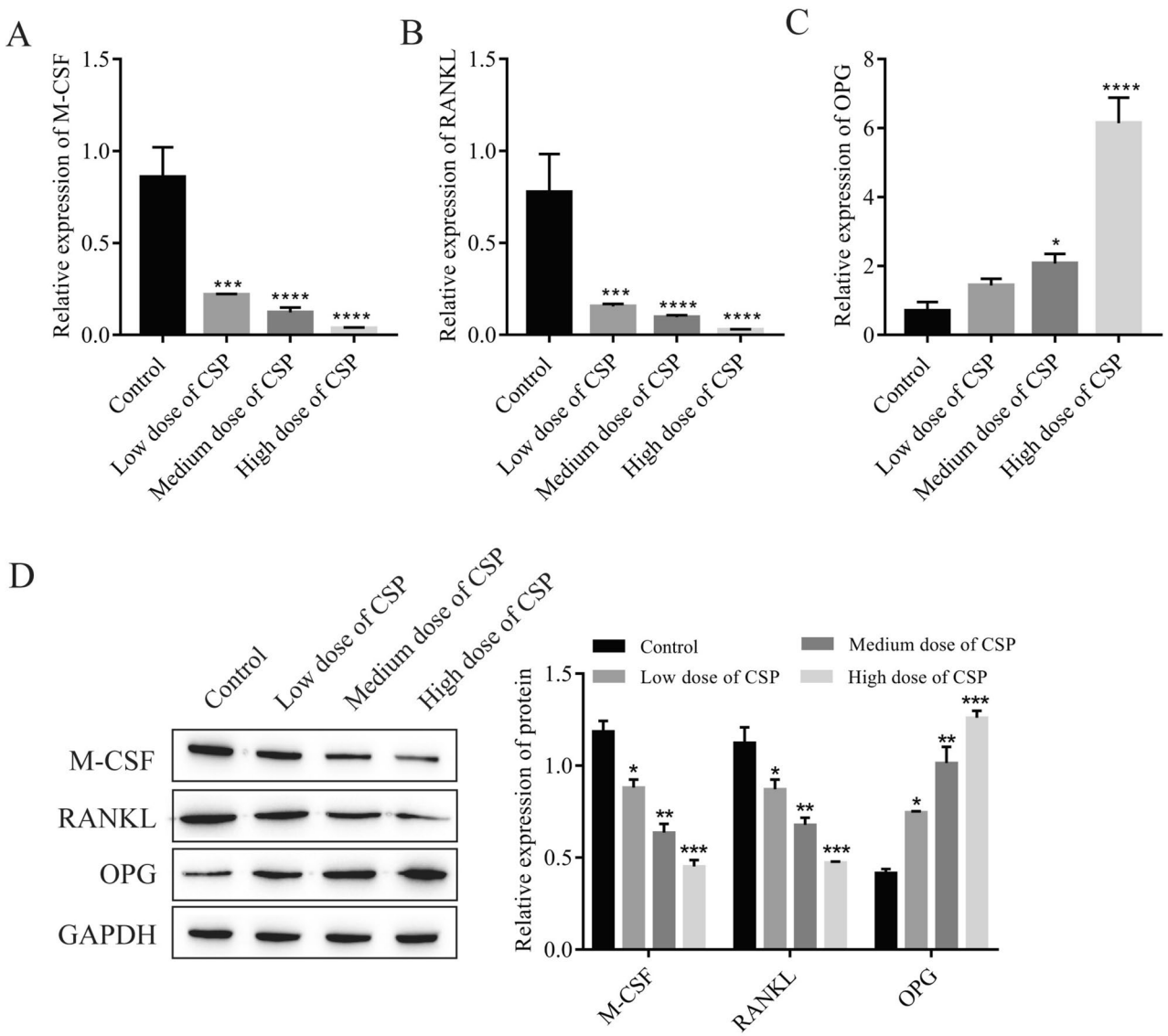

Figure 3. CSP regulates the OPG/RANKL/RANK signaling pathway in BMSCs ($n=3$). (*A–C*) The expression of M-CSF, RANKL, and OPG was detected by RT-qPCR. (*D*) The protein expression of M-CSF, RANKL, and OPG was detected by Western blot analysis. $^{*}P<0.5$, $^{**}P<0.01$, $^{***}P<0.001$, $^{****}P<0.0001$ vs. control. Cells were incubated with CSP for 48 h. Low, medium, and high doses of CPS refer to 0.4 mg/L, 4 mg/L, and 40 mg/L CPS, respectively.

washed with PBS, and incubated with 0.5% Triton X-100 penetrant on a shaker for 10 min. Following an additional wash with PBS, the cells were stained with the preprepared Apollo staining solution, destained, incubated in the dark on a shaker for 30 min, and washed with PBS. Next, nuclei were stained with 10 μL of 4′,6-diamidino-2-phenylindole (DAPI) in the dark for 30 min and washed with PBS, and image acquisition was performed under a fluorescence microscope.

Cell apoptosis assay Flow cytometry was used to measure apoptosis. After the different groups of cells were treated, the cells were collected in a flow tube, centrifuged at 4°C, washed with PBS, and resuspended. The cells were incubated according to the instructions for the Annexin V Combined Fluorescein Isothiocyanate/Propidium Iodide Kit (Abcam), and then Annexin V and PI fluorescence were detected at the referenced emission wavelengths using a flow cytometer (BD Biosciences) and FlowJo software.

TRAP staining For TRAP staining, slides containing cells were rinsed with PBS, fixed, and rinsed with deionized water at 25°C for 30 s. The cells were heated in a water bath to 37°C, immersed in staining solution, and incubated at 37°C for 1 h in the dark. They were then rinsed with deionized

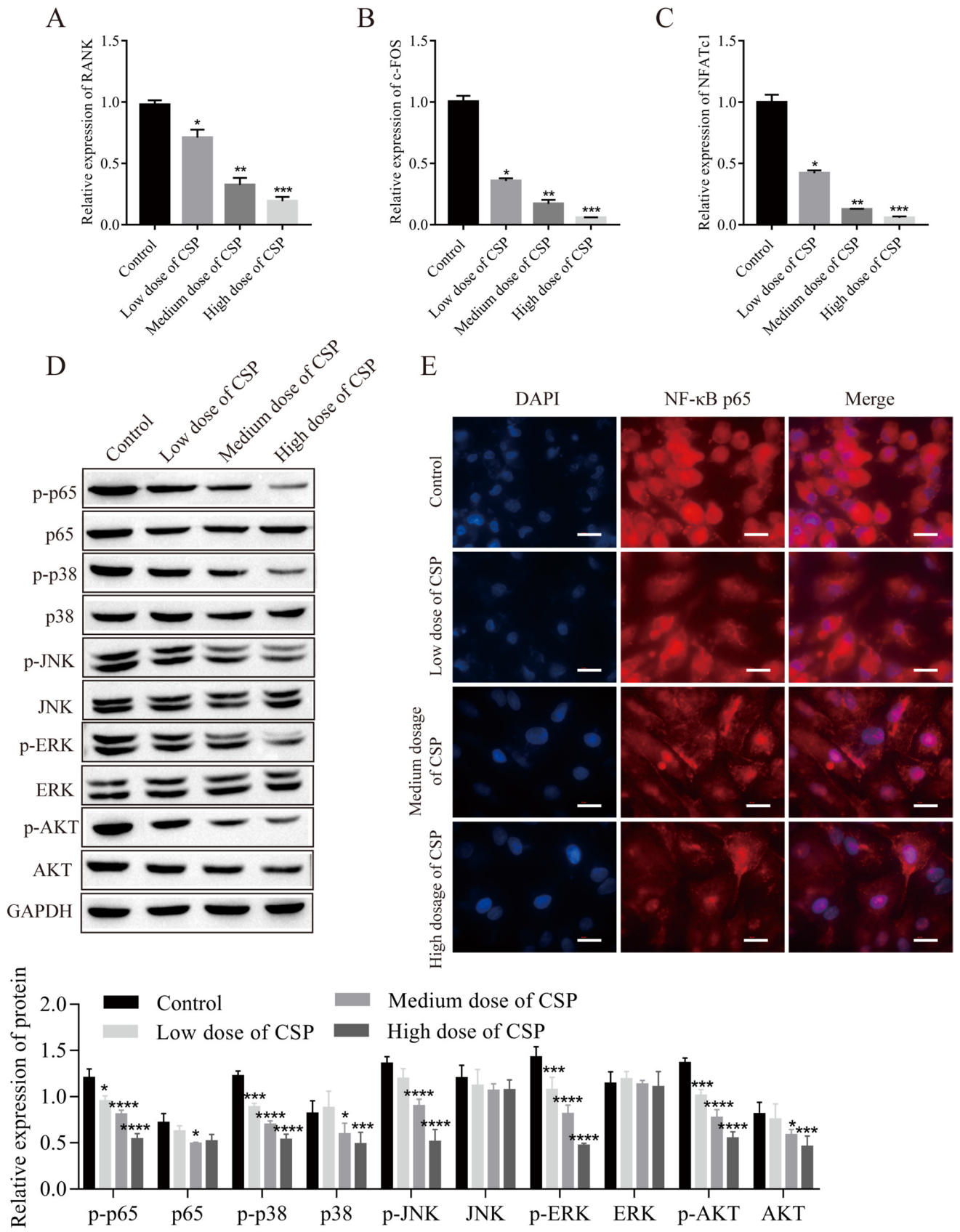
A
Relative expression of RANK
1.5
1.0
0.5
0.0
*
**
***
Control
Low dose of CSP
Medium dose of CSP
High dose of CSP
B
Relative expression of c-FOS
1.5
1.0
0.5
0.0
*
**
***
Control
Low dose of CSP
Medium dose of CSP
High dose of CSP
C
Relative expression of NFATc1
1.5
1.0
0.5
0.0
*
**
***
Control
Low dose of CSP
Medium dose of CSP
High dose of CSP
D
Control
Low dose of CSP
Medium dose of CSP
High dose of CSP
p-p65
p65
p-p38
p38
p-JNK
JNK
p-ERK
ERK
p-AKT
AKT
GAPDH
E
DAPI
NF-κB p65
Merge
Control
Low dose of CSP
Medium dosage of CSP
High dosage of CSP
Relative expression of protein
2.0
1.5
1.0
0.5
0.0
Control
Low dose of CSP
Medium dose of CSP
High dose of CSP
p-p65
p65
p-p38
p38
p-JNK
JNK
p-ERK
ERK
p-AKT
AKT

◂**Figure 4.** CSP inhibits the activation of NF-κB by inhibiting the RANKL-RANK signaling pathway in RAW264.7 cells ($n=3$). (*A–C*) The expression of RANK, NFATc1, and c-FOS was detected by RT-qPCR. (*D*) Protein expression was detected by Western blot analysis. (*E*) Nuclear translocation of NF-κB p65 was detected by immunofluorescence analysis (*scale bar*=20 μm). $*P<0.5$, $**P<0.01$, $***P<0.001$ vs. control. Cells were incubated with CSP for 48 h. Low, medium, and high doses of CPS refer to 0.4 mg/L, 4 mg/L, and 40 mg/L CPS, respectively.

water, counterstained with hematoxylin for 90 s, rinsed with alkaline solution for several minutes, and observed under a microscope after being dried. For rat femur TRAP staining, after the paraffin sections were dewaxed, they were dipped in staining solution that was prewarmed to 37°C for 1 h, rinsed with distilled water, dehydrated with gradient alcohol, cleared with xylene, and sealed with neutral gum, and osteoclasts were observed under a microscope.

Immunofluorescence analysis of NF-κB/p65 nuclear translocation The NF-κB nuclear translocation assay was performed according to the instructions of the Nuclear Translocation Assay Kit (SN368, Beyotime). The cells were centrifuged to remove the culture medium, washed with PBS, and fixed with fixative for 5–15 min. After the fixative was removed, immunostaining blocking solution was added and incubated at 25°C for 1 h. The immunostaining blocking solution was aspirated, and the NF-κB p65 antibody was added and incubated for 1 h. After the primary antibody was removed, anti-rabbit Cy3 was added and incubated at room temperature for 1 h. After the samples were stained with DAPI for 15 min, images were acquired under a fluorescence microscope.

Development of the oophorectomy (OVX) rat model Six-month-old female SD rats were used to construct the model, and 5 groups were assigned: the sham operation group (sham), oophorectomy model group (OVX), CSP (Xiang Cao Biotechnology Ltd, Ningxia, China) low-dose treatment group (L-CSP), CSP medium-dose treatment group (M-CSP), and CSP high-dose treatment group (H-CSP). After 2 wk of adaptive feeding, a postmenopausal osteoporosis model was established according to the classic modeling method. In the sham group, 1% pentobarbital sodium (30 mg/kg body weight) was injected into the abdominal cavity, and anesthetized animals were fixed in the prone position. Under aseptic conditions, a dorsal median incision was performed to open the abdominal cavity near the lower abdomen, and the ovaries were identified. Fat tissue around the ovaries with the same weight as the bilateral ovaries was removed, and the incision was sutured in layers. In the OVX group, 1% pentobarbital sodium (30 mg/kg) was injected into the abdominal cavity, and the anesthetized animals were fixed in the prone position. Under aseptic conditions, a dorsal median incision was performed to open the abdominal cavity near the lower abdomen, the bilateral ovaries were identified and removed, and the incision was stitched in layers. In the L-CSP group, bilateral oophorectomy was performed as described in the model group, and 10 mg/kg CSP was administered orally every day beginning on the 7th day after surgery. In the M-CSP group, bilateral oophorectomy was performed as described in the model group, and 40 mg/kg CSP was administered orally every day beginning on the 7th day after surgery. In the H-CSP group, bilateral oophorectomy was performed as described in the model group, and 160 mg/kg CSP was administered orally every day beginning on the 7th day after surgery. Treatment was continued for 90 d. Rat femurs were collected for subsequent analysis.

Enzyme-linked immunosorbent assay (ELISA) Plates containing standard substances and serum samples from each group were incubated at 37℃ for 1 h and then washed with wash solution. Next, 50 μL of HRP-antibody solution was added to each cell well and incubated at 37℃ for 30 min and washed, followed by the addition of 50 μL substrate A and substrate B, incubation at 37℃ in the dark for 15 min, addition of 50 μL stop solution/well, and measurement of the OD value at a wavelength of 450 nm within 30 min.

Hematoxylin–eosin (H&E) staining Rat femurs were fixed for 48 h and then decalcified with 10% EDTA solution at room temperature for 6 wk. Femurs approximately 1 cm in length were dehydrated in a graded ethanol series (70%, 80%, 90%, 95%, 100%×3, soaking in each solution for 60–70 min). Xylene (2 lanes, total 60 min) and immersion wax (3 lanes, total 70 min) were then applied. Paraffin-embedded sections were obtained using routine procedures. After being dewaxed with xylene, the sections were soaked in hematoxylin staining solution for 3 min, rinsed with tap water for 10 min, differentiated with 1% hydrochloric acid and ethanol for several seconds, rinsed again with running water for 10 min until the blue color was restored, stained with eosin staining solution for 3 min, and rinsed for 10 min. Transparent xylene and neutral resin mounts were observed under a microscope and photographed.

Statistical analysis The data are presented as the mean ± SD. For statistical comparisons, Student's *t* test was used to compare two groups, and one-way ANOVA was performed for multiple groups. All cell experiments were performed with 3 parallel experiments, and each parallel experiment included 3 replicates. The animal experiment was performed in 5 parallel experiments.

Results

CSP promoted apoptosis in RAW264.7 cells In this study, different concentrations of CSP had an inhibitory effect on RAW264.7 cells (Fig. 1*A*, *B*). The protein expression of

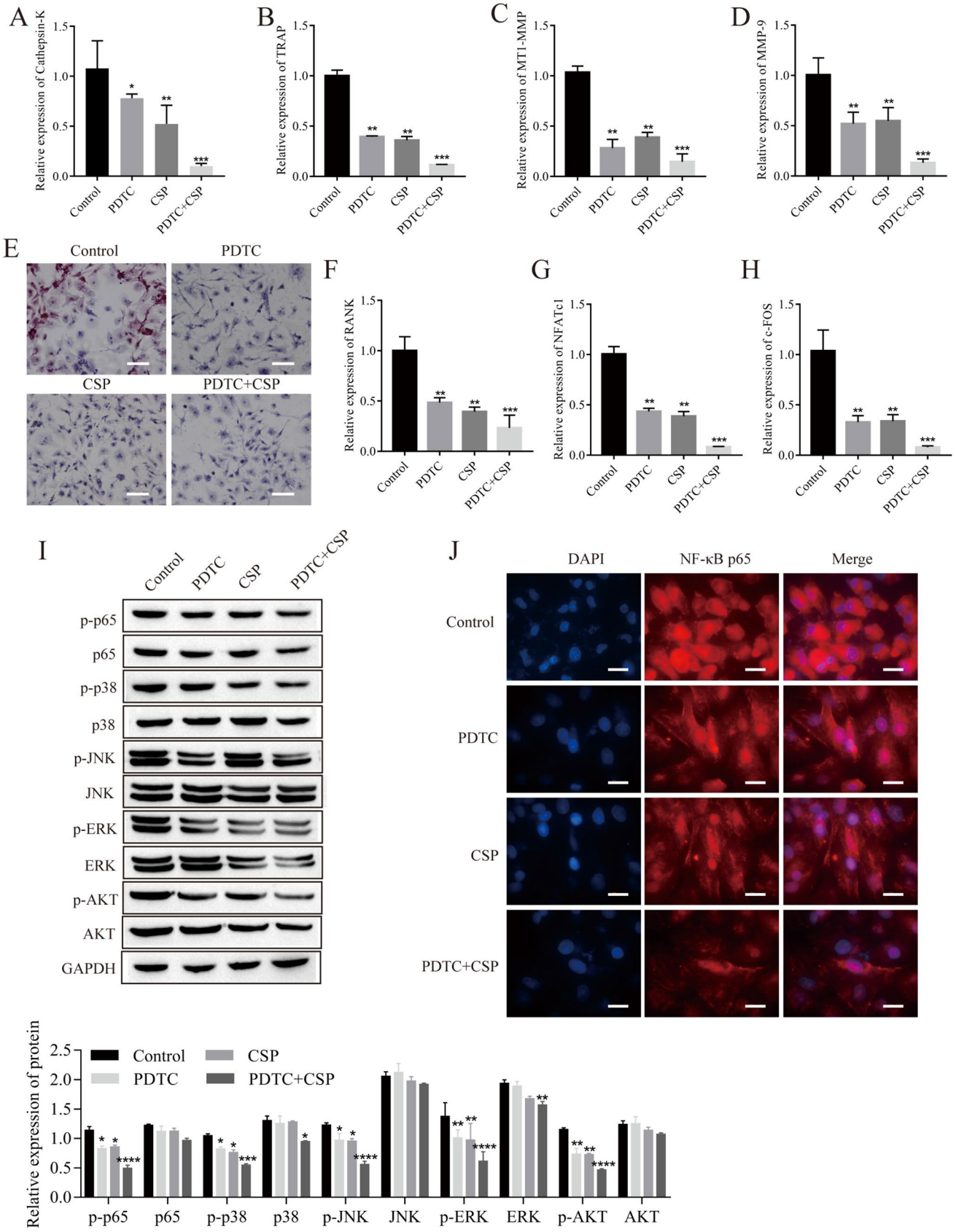
A
Relative expression of Cathepsin-K
B
Relative expression of TRAP
C
Relative expression of MT1-MMP
D
Relative expression of MMP-9
Control
PDTC
CSP
PDTC+CSP
E
F
Relative expression of RANK
G
Relative expression of NFATc1
H
Relative expression of c-FOS
I
p-p65
p65
p-p38
p38
p-JNK
JNK
p-ERK
ERK
p-AKT
AKT
GAPDH
J
DAPI
NF-κB p65
Merge
Relative expression of protein

◂**Figure 5.** CSP enhances the inhibitory effect of PDTC on osteoclast formation and downstream signaling pathway activation in RAW264.7 cells ($n=3$). (*A–D*) The expression levels of Cathepsin-K, TRAP, MT1-MMP, and MMP-9 were detected by RT-qPCR. (*E*) The number of positive multinucleated giant cells was detected by TRAP staining (scale bar=100 μm). (*F–H*) The expression of RANK, NFATc1, and c-FOS was detected by RT-qPCR. (*I*) Protein expression was detected by Western blot analysis. (*J*) Nuclear translocation of NF-κB p65 was detected by immunofluorescence analysis (*scale bar*=20 μm). $^{*}P<0.5$, $^{**}P<0.01$, $^{***}P<0.001$, $^{****}P<0.0001$ vs. control. Cells were incubated with CSP (40 mg/L) or PDTC (4 μmol/L) for 48 h.

Bcl-2 in the CSP treatment group was downregulated, and the protein expression levels of Bax and Caspase-3 were upregulated; a more pronounced effect was observed in response to a higher concentration of CSP (Fig. 1*C*). Flow cytometry revealed that increasing CSP concentrations resulted in higher rates of apoptosis (Fig. 1*D*).

CSP inhibits osteoclast formation in a dose-dependent manner The effects of different concentrations of CSP on the formation of osteoclasts were observed. RT-qPCR showed that the expression levels of the osteoclast-related genes Cathepsin-K, TRAP, MT1-MMP, and MMP-9 were downregulated in the CSP-treated group in a dose-dependent manner (Fig. 2*A–D*). Based on the TRAP staining results, the number of TRAP-positive multinucleated giant cells in the CSP group decreased with increasing CSP concentrations (Fig. 2*E*).

CSP regulates the OPG/RANKL/RANK pathway The levels of OPG/RANKL/RANK pathway–related proteins in BMSCs treated with different concentrations of CSP were detected. The expression levels of M-CSF and RANKL gradually decreased, and the levels of OPG gradually increased with increasing CSP concentrations (Fig. 3*A–C*). The western blot results were consistent with the RT-qPCR results (Fig. 3*D*).

CSP inhibits the activation of NF-κB by inhibiting the RANKL-RANK signaling pathway The effects of CSP on the NF-κB pathway were examined and showed a gradual decrease in RANK, NFATc1, and c-Fos expression with increasing CSP concentrations (Fig. 4*A–C*). The phosphorylation levels of p65, p38, ERK, JNK, and AKT were decreased after CSP treatment (Fig. 4*D*). Concurrently, an immunofluorescence assay was used to examine the nuclear translocation of NF-κB p65, and the expression of p65 in the nucleus decreased with increasing CSP concentrations (Fig. 4*E*).

CSP enhances the inhibitory effect of PDTC on osteoclast formation and downstream signaling pathway activation Cells were treated with PDTC, an inhibitor of the NF-κB signaling pathway, which inhibited osteoclast formation, and CSP enhanced the inhibitory effect of PDTC on osteoclast formation. The expression of the osteoclast-related genes Cathepsin-K, TRAP, MT1-MMP, and MMP-9 was downregulated in the PDTC group. The same effect was observed in the PDTC + CSP group, and the degree of downregulation was greater than that in the PDTC group (Fig. 5*A–D*). Furthermore, there were fewer TRAP-positive multinucleated giant cells in the PDTC group than in the control group, and there were fewer TRAP-positive multinucleated giant cells in the PDTC + CSP group than the PDTC group (Fig. 5*E*). In addition, PDTC inhibited the activation of downstream signaling pathways, and this effect was enhanced by CSP. In the PDTC group, the RT-qPCR results showed downregulated expression of RANK, NFATc1, and C-FOS, and the degree of the downregulation was increased in the PDTC + CSP group (Fig. 5*F–H*). The phosphorylation levels of p65, P38, ERK, JNK, and AKT were downregulated, and the degree of the downregulation was greater in the PDTC + CSP group (Fig. 5*I*). The immunofluorescence results revealed a reduction in nuclear expression of NF-κB p65 in the PDTC group and even lower nuclear expression in the PDTC + CSP group (Fig. 5*J*).

CSP ameliorates bone structure loss in rats Serum levels of OPG, RANKL, and M-CSF in rats were detected by ELISA. The results showed that compared with that in the sham group, the expression of OPG was downregulated and the expression of RANKL and M-CSF was upregulated in the OVX group. However, after treatment with different concentrations of CSP, the expression of OPG increased, while the expression of RANKL and M-CSF was inhibited, and this effect was strongest in the H-CSP group (Fig. 6*A–C*). Compared with those in the sham group, the expression levels of RANK, NF-κB, NFATc1, and c-Fos were upregulated in the OVX group; these expression levels were downregulated in the CSP group; and the degree of downregulation was greatest in the H-CSP group (Fig. 6*D*). H&E staining showed that the trabecular bones of rats in the sham group had uniform thickness, complete structures, and small spaces. Rats in the OVX group showed numerous changes, such as a larger bone marrow cavity, thinner trabecular bone, and enlarged space, and the overall structure was severely altered. Treatment with CSP improved the lack of bone structure in rats. In the H-CSP group, the boundary between cortical bone and bone marrow was clear, and the structure was complete and almost normal (Fig. 6*E*). In the OVX group, TRAP staining revealed an increase in irregularly located wine-red osteoclasts at the edge of the trabecular bone, and osteoclasts dose-dependently decreased in the L-CSP, M-CSP, and H-CSP groups (Fig. 6*F*). Compared with those in the sham group, the bone mineral density (BMD), bone volume fraction (bone volume/total volume, BV/TV), trabecular number (Tb.N), and connectivity density (Conn. D) in the

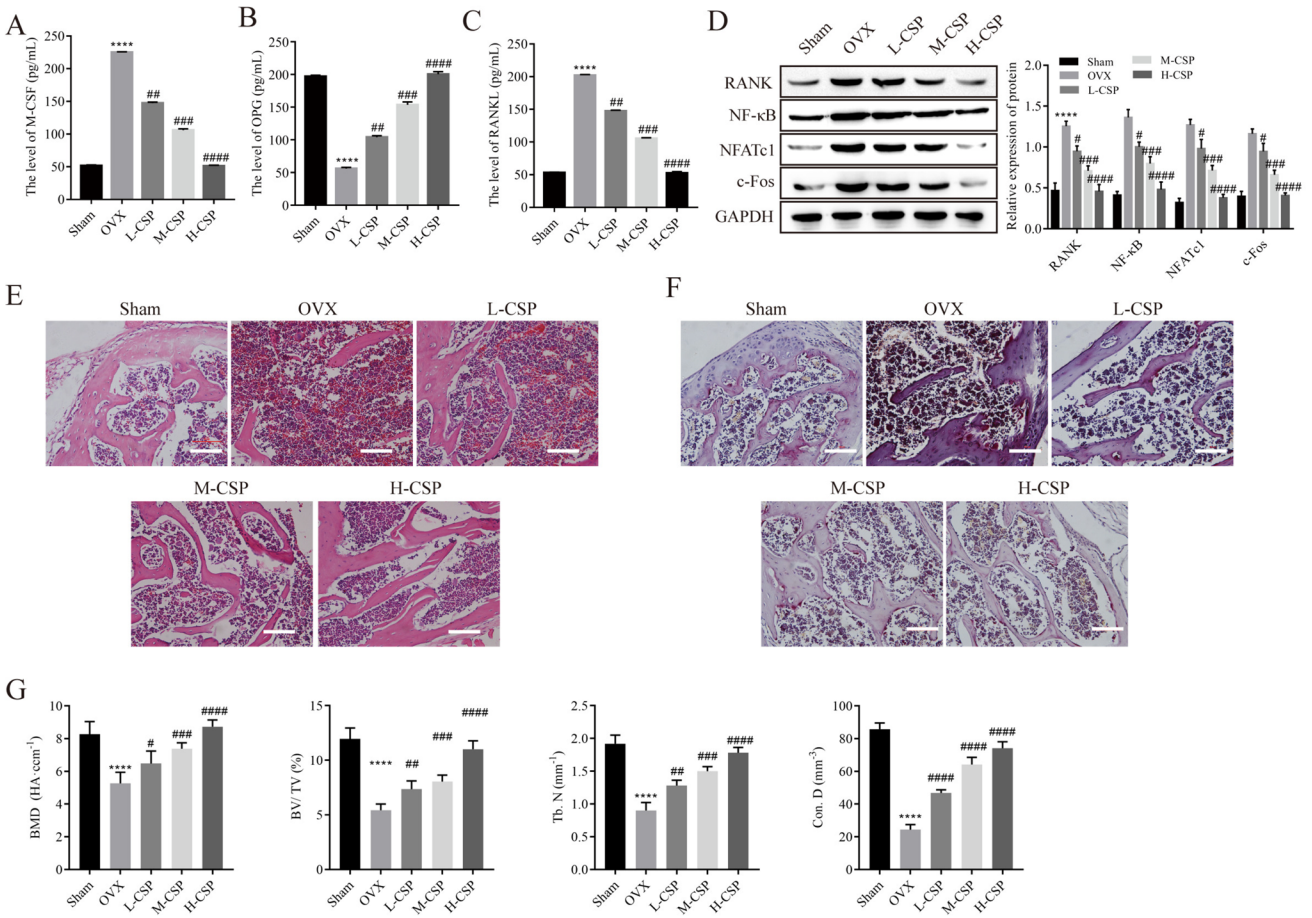

Figure 6. CSP ameliorates bone structure loss in rats ($n=5$). (*A–C*) The expression levels of M-CSF, OPG, and RANKL were detected by ELISA. (*D*) Protein expression was detected by Western blot analysis. (*E*) The effect of CSP on bone structure observed by H&E staining (*scale bar*=100 μm). (*F*) The effect of CSP on osteoclast formation observed by TRAP staining (*scale bar*=100 μm). (*G*) Quantitative analysis of BMD, BV/TV, Tb. N, and Conn. D in each group of rats. $^{****}P<0.0001$ vs. control; $^{\#\#}P<0.01$, $^{\#\#\#}P<0.001$, $^{\#\#\#\#}P<0.0001$ vs. OVX. Low, medium, and high doses of CPS refer to 10 mg/kg/d, 40 mg/kg/d, and 100 mg/kg/d CPS, respectively. BMD, bone mineral density; BV/TV, bone volume/total volume; Tb. N, trabecular number; Conn. D, connectivity density.

OVX group were significantly decreased, indicating successful modeling. BMD, BV/TV, Tb.N and Conn. D were significantly increased by the administration of CSP, and the therapeutic effect in the high-dose group was significantly better than that in the low- and medium-dose groups (Fig. 6*G*). These results suggest that CSP can protect against bone microstructural damage induced by OVX.

Discussion

In postmenopausal women, bone resorption is greater than bone formation due to declines in ovarian function and estrogen levels, resulting in systemic osteopenia and destruction of the bone microstructure (McClung *et al*. 2017). In addition, an important factor in osteopenia is the imbalance between osteoclast-driven bone resorption and osteoblast-driven bone formation (Dimitriou *et al*. 2011; Cui *et al*. 2019). Studies have shown that the active ingredients in natural traditional Chinese medicines can reduce degradation of the bone microstructure to maintain the balance of bone resorption (An *et al*. 2016). Thus, studies of the related mechanisms of these components for osteoporosis drug treatment are meaningful.

Previous research has demonstrated that natural compounds have great potential in the treatment of osteoporosis (Tao *et al*. 2018). For example, RANKL-induced osteoclast differentiation and maturation can be inhibited by hesperetin (Hes) from citrus fruits, which has protective effects on osteoporotic animals (Zhang *et al*. 2018). As a raw material for separating peptides, cucumber seeds are widely used in the field of modern Chinese medicine and can supplement calcium, strengthen bones, and treat osteoporosis. This study showed that CSP inhibited RANKL-induced osteoclastogenesis in a concentration-dependent manner. Moreover, bone remodeling requires intimate cross-talk between osteoclasts

and osteoblasts (Kular *et al*. 2012), and bone homeostasis depends on the resorption of bone by osteoclasts and the formation of bone by osteoblasts (Chen *et al*. 2018). In this study, CSP inhibited osteoclast differentiation and maintained bone homeostasis by regulating the expression of M-CSF, RANKL, and OPG in the OVX model, and CSP ameliorated bone structure loss in OVX rats. This study confirmed that the cucumber seed extract CSP alleviated the symptoms of osteoporosis in rats by mediating osteoclastic and osteoblastic bone differentiation in vivo.

OPG/RANL/RANK is an important signaling pathway that regulates the differentiation and induction of osteoclasts, which can directly or indirectly affect senile and postmenopausal osteoporosis (Udagawa *et al*. 2021; Zhao *et al*. 2020). OPG and RANK are receptors of RANKL. On the surface of osteoclasts, the binding of RANKL to RANK stimulates the activation of osteoclasts, while OPG can block binding of RANKL to RANK to inhibit bone resorption (Maria *et al*. 2018; Yasuda *et al*. 1998). M-CSF is also a key factor in osteoclast formation, and the M-CSF signaling pathway induces osteoclast proliferation and maintains osteoclast survival. In our study, CSP inhibited the expression of M-CSF and RANKL and promoted the expression of OPG by regulating the OPG/RANKL/RANK pathway while inhibiting the osteoclast-associated genes MT1-MMP, TRAP, MMP-9, and Cathepsin-K, which have been reported to be markers associated with osteoclast differentiation and function (Junrui *et al*. 2016).

After RANKL binds to RANK, downstream signaling pathways are activated, mainly through RANK-induced ubiquitination of the junction molecule TRAF6, which is involved in osteoclast differentiation and activation of the NF-κB, PI3K/Akt, and MAPK (P38, ERK, JNK) pathways (Boyle *et al*. 2003; He *et al*. 2014). Activation of NF-κB signaling results in the nuclear translocation and phosphorylation of NF-κB p65, which contributes to osteoclast maturation and enhances bone resorption activity (Ding *et al*. 2022). In addition, the NF-κB pathway has multiple regulatory effects on osteoclastogenesis, and abnormal activation of NF-κB signaling in osteoclasts is related to osteoclast activity. For instance, NF-κB modulators such as parthenolide and NEMO-binding domain peptide exert therapeutic effects on inflammation-induced bone destruction in mouse models (Xu *et al*. 2009). In the present study, we found that CSP significantly reduced the protein expression of AKT, P65, ERK, P38, and JNK; inhibited downstream signaling pathway activation; and inhibited nuclear NF-κB p65 translocation. These results indicate that abnormal activation of the NF-κB signaling pathway in osteoclasts is closely related to the activity of osteoclasts, and the inhibitory effect of CSP on the NF-κB pathway in osteoclasts is critical for the treatment of postmenopausal osteoporosis. In addition, CSP enhanced the expression of osteoclast effector genes, which are functional molecules in osteoclast development. Among these osteoclast effector genes, NFATC-1 is considered to be an important regulator of enhanced osteoclast formation (Boyce *et al*. 2015). In addition, defective expression of c-Fos, a key transcription factor that affects osteoclast differentiation, in mice leads to severe osteosclerosis due to complete blockade of osteoclast differentiation (Matsuo *et al*. 2000; Wagner and Eferl 2005). In this study, we found that with increasing CSP concentrations, the expression of NFATc1 and c-Fos in RANKL-induced RAW264.7 cells gradually decreased.

Conclusion

Overall, the current findings show that CSP can inhibit RANKL-induced osteoclast formation and ameliorate bone structure loss in rats. These effects are mainly achieved through regulating the OPG/RANKL/RANK pathway and inhibiting the NF-kB pathway.. Therefore, CSP is a potential treatment for postmenopausal osteoporosis, although its clinical application requires further research.

Author contribution Conceptualization: Tao Yu and Xiao Liu; methodology: Tao Yu, Xiao Liu, and Meng Jiang; software: Xiao Liu and Yuanyue Li; validation: Meng Jiang and Heng Su; formal analysis: Tao Yu, Xiao Liu, and Ben Niu; investigation: Tao Yu and Ben Niu; resources: Ben Niu; data curation: Tao Yu, Meng Jiang, and Heng Su; writing—original draft preparation: Tao Yu, Xiao Liu, Meng Jiang, and Yuanyue Li; writing—review and editing: Tao Yu, Heng Su, and Ben Niu; visualization: Tao Yu and Ben Niu; supervision: Ben Niu; funding acquisition: Ben Niu. All authors have read and agreed to the published version of the manuscript.

Funding This study was supported by the Joint Special Fund Project of Yunnan Provincial Science and Technology Department and Kunming Medical University for Applied Basic Research (grant number: 2019FE001), Yunnan Province Young and Middle-Aged Academic and Technical Leaders Reserve Talents Project (grant number: 202105AC160028), Dong Birong Expert Workstation of Yunnan Province (grant number: 202105AF150032), and Clinical Medical Research Center for Geriatric Disease of Yunnan Province (grant number: 202102AA310002), Yunnan Xingdian Talents Support Program "Medical and Health Talents Special Project".

Data availability The datasets used and/or analyzed in the current study are available from the corresponding author upon reasonable request.

Declarations

Compliance with ethical standards We declare that the in vivo vertebrate experiments in this study were approved by the Animal Ethics Review Committee of Kunming University of Science and Technology. All experiments were carried out in accordance with the relevant guidelines and regulations.

Informed consent Not applicable.

Competing interests The authors declare no competing interests.

References

An J, Yang H, Zhang Q, Liu C, Zhao J, Zhang L, Chen B (2016) Natural products for treatment of osteoporosis: the effects and mechanisms on promoting osteoblast-mediated bone formation. Life Sci 147:46–58. https://doi.org/10.1016/j.lfs.2016.01.024

Anudeep S, Prasanna VK, Adya SM, Radha C (2016) Characterization of soluble dietary fiber from Moringa oleifera seeds and its immunomodulatory effects. Int J Biol Macromol 91:656–662. https://doi.org/10.1016/j.ijbiomac.2016.06.013

Arceo-Mendoza RM, Camacho PM (2021) Postmenopausal osteoporosis: latest guidelines. Endocrinol Metab Clin North Am 50:167–178. https://doi.org/10.1016/j.ecl.2021.03.009

Boyce BF, Xiu Y, Li J, Xing L, Yao Z (2015) NF-Kb-mediated regulation of osteoclastogenesis. Endocrinol Metab (Seoul) 30:35–44. https://doi.org/10.3803/EnM.2015.30.1.35

Boyle WJ, Simonet WS, Lacey DL (2003) Osteoclast differentiation and activation. Nature 423:337–342. https://doi.org/10.1038/nature01658

Brown JP (2021) Long-term treatment of postmenopausal osteoporosis. Endocrinol Metab (Seoul) 36:544–552. https://doi.org/10.3803/EnM.2021.301

Chen K, Yan Z, Wang Y, Yang Y, Cai M, Huang C, Li B, Yang M, Zhou X, Wei X, Yang C, Chen Z, Zhai X, Li M (2020) Shikonin mitigates ovariectomy-induced bone loss and RANKL-induced osteoclastogenesis via TRAF6-mediated signaling pathways. Biomed Pharmacother 126:110067. https://doi.org/10.1016/j.biopha.2020.110067

Chen X, Wang Z, Duan N, Zhu G, Schwarz EM, Xie C (2018) Osteoblast-osteoclast interactions. Connect Tissue Res 59:99–107. https://doi.org/10.1080/03008207.2017.1290085

Cui Z, Meng X, Feng H, Zhuang S, Liu Z, Zhu T, Ye K, Xing Y, Sun C, Zhou F, Tian Y (2019) Estimation and projection about the standardized prevalence of osteoporosis in mainland China. Arch Osteoporos 15:2. https://doi.org/10.1007/s11657-019-0670-6

Dimitriou R, Jones E, McGonagle D, Giannoudis PV (2011) Bone regeneration: current concepts and future directions. BMC Med 9:66. https://doi.org/10.1186/1741-7015-9-66

Ding D, Yan J, Feng G, Zhou Y, Ma L, Jin Q (2022) Dihydroartemisinin attenuates osteoclast formation and bone resorption via inhibiting the NF-κB, MAPK and NFATc1 signaling pathways and alleviates osteoarthritis. Int J Mol Med 49. https://doi.org/10.3892/ijmm.2021.5059

Dong C, Liu X, Li J, Lan D, Zheng S (2022) Dysregulation of the HOTAIR-miR-152-CAMKIIα axis in craniosynostosis results in impaired osteoclast differentiation. Front Genet 13:787734. https://doi.org/10.3389/fgene.2022.787734

Feng S, Wang H, Yan Y, Su X, Ao J, Chen W (2021) Regulatory SNP of RREB1 is associated with bone mineral density in Chinese postmenopausal osteoporosis patients. Front Genet 12:756957. https://doi.org/10.3389/fgene.2021.756957

He Y, Zhang Q, Shen Y, Chen X, Zhou F, Peng D (2014) Schisantherin A suppresses osteoclast formation and wear particle-induced osteolysis via modulating RANKL signaling pathways. Biochem Biophys Res Commun 449:344–350. https://doi.org/10.1016/j.bbrc.2014.05.034

Junrui P, Bingyun L, Yanhui G, Xu J, Darko GM, Dianjun S (2016) Relationship between fluoride exposure and osteoclast markers during RANKL-induced osteoclast differentiation. Environ Toxicol Pharmacol 46:241–245. https://doi.org/10.1016/j.etap.2016.08.001

Kovács B, Vajda E, Nagy EE (2019) Regulatory effects and interactions of the Wnt and OPG-RANKL-RANK signaling at the bone-cartilage interface in osteoarthritis. Int J Mol Sci 20. https://doi.org/10.3390/ijms20184653

Kular J, Tickner J, Chim SM, Xu J (2012) An overview of the regulation of bone remodelling at the cellular level. Clin Biochem 45:863–873. https://doi.org/10.1016/j.clinbiochem.2012.03.021

Lin ZM, Liu YT, Xu YS, Yang XQ, Zhu FH, Tang W, He SJ, Zuo JP (2019) Cervus and cucumis peptides ameliorates bone erosion in experimental arthritis by inhibiting osteoclastogenesis. Lupus Sci Med 6:e000331. https://doi.org/10.1136/lupus-2019-000331

Lloyd SA, Yuan YY, Kostenuik PJ, Ominsky MS, Lau AG, Morony S, Stolina M, Asuncion FJ, Bateman TA (2008) Soluble RANKL induces high bone turnover and decreases bone volume, density, and strength in mice. Calcif Tissue Int 82:361–372. https://doi.org/10.1007/s00223-008-9133-6

Ma B, Zhang Q, Wu D, Wang YL, Hu YY, Cheng YP, Yang ZD, Zheng YY, Ying HJ (2012) Strontium fructose 1,6-diphosphate prevents bone loss in a rat model of postmenopausal osteoporosis via the OPG/RANKL/RANK pathway. Acta Pharmacol Sin 33:479–489. https://doi.org/10.1038/aps.2011.177

Maria S, Samsonraj RM, Munmun F, Glas J, Silvestros M, Kotlarczyk MP, Rylands R, Dudakovic A, van Wijnen AJ, Enderby LT, Lassila H, Dodda B, Davis VL, Balk J, Burow M, Bunnell BA, Witt-Enderby PA (2018) Biological effects of melatonin on osteoblast/osteoclast cocultures, bone, and quality of life: implications of a role for MT2 melatonin receptors, MEK1/2, and MEK5 in melatonin-mediated osteoblastogenesis. J Pineal Res 64. https://doi.org/10.1111/jpi.12465

Matsuo K, Owens JM, Tonko M, Elliott C, Chambers TJ, Wagner EF (2000) Fosl1 is a transcriptional target of c-Fos during osteoclast differentiation. Nat Genet 24:184–187. https://doi.org/10.1038/72855

McClung MR, Lippuner K, Brandi ML, Zanchetta JR, Bone HG, Chapurlat R, Hans D, Wang A, Zapalowski C, Libanati C (2017) Effect of denosumab on trabecular bone score in postmenopausal women with osteoporosis. Osteoporos Int 28:2967–2973. https://doi.org/10.1007/s00198-017-4140-y

McDonald MM, Khoo WH, Ng PY, Xiao Y, Zamerli J, Thatcher P, Kyaw W, Pathmanandavel K, Grootveld AK, Moran I, Butt D, Nguyen A, Corr A, Warren S, Biro M, Butterfield NC, Guilfoyle SE, Komla-Ebri D, Dack MRG, Dewhurst HF, Logan JG, Li Y, Mohanty ST, Byrne N, Terry RL, Simic MK, Chai R, Quinn JMW, Youlten SE, Pettitt JA, Abi-Hanna D, Jain R, Weninger W, Lundberg M, Sun S, Ebetino FH, Timpson P, Lee WM, Baldock PA, Rogers MJ, Brink R, Williams GR, Bassett JHD, Kemp JP, Pavlos NJ, Croucher PI, Phan TG (2021) Osteoclasts recycle via osteomorphs during RANKL-stimulated bone resorption. Cell 184:1330-1347.e1313. https://doi.org/10.1016/j.cell.2021.02.002

McNamara LM (2010) Perspective on post-menopausal osteoporosis: establishing an interdisciplinary understanding of the sequence

of events from the molecular level to whole bone fractures. J R Soc Interface 7:353–372. https://doi.org/10.1098/rsif.2009.0282

Mohan A, McClements DJ, Udenigwe CC (2016) Encapsulation of bioactive whey peptides in soy lecithin-derived nanoliposomes: influence of peptide molecular weight. Food Chem 213:143–148. https://doi.org/10.1016/j.foodchem.2016.06.075

Rajapakse N, Mendis E, Byun HG, Kim SK (2005) Purification and in vitro antioxidative effects of giant squid muscle peptides on free radical-mediated oxidative systems. J Nutr Biochem 16:562–569. https://doi.org/10.1016/j.jnutbio.2005.02.005

Shen S, Wang W, Yang C, Xu B, Zeng L, Qian Y (2019) Effect of technetium-99 conjugated with methylene diphosphonate ((99) Tc-MDP) on OPG/RANKL/RANK system in vitro. J Oral Pathol Med 48:129–135. https://doi.org/10.1111/jop.12801

Tao X, Yin L, Xu L, Peng J (2018) Dioscin: a diverse acting natural compound with therapeutic potential in metabolic diseases, cancer, inflammation and infections. Pharmacol Res 137:259–269. https://doi.org/10.1016/j.phrs.2018.09.022

Udagawa N, Koide M, Nakamura M, Nakamichi Y, Yamashita T, Uehara S, Kobayashi Y, Furuya Y, Yasuda H, Fukuda C, Tsuda E (2021) Osteoclast differentiation by RANKL and OPG signaling pathways. J Bone Miner Metab 39:19–26. https://doi.org/10.1007/s00774-020-01162-6

Wagner EF, Eferl R (2005) Fos/AP-1 proteins in bone and the immune system. Immunol Rev 208:126–140. https://doi.org/10.1111/j.0105-2896.2005.00332.x

Wang X, Gao A, Chen Y, Zhang X, Li S, Chen Y (2017) Preparation of cucumber seed peptide-calcium chelate by liquid state fermentation and its characterization. Food Chem 229:487–494. https://doi.org/10.1016/j.foodchem.2017.02.121

Wei J, Wang J, Gong Y, Zeng R (2015) Effectiveness of combined salmon calcitonin and aspirin therapy for osteoporosis in ovariectomized rats. Mol Med Rep 12:1717–1726. https://doi.org/10.3892/mmr.2015.3637

Xu J, Wu HF, Ang ES, Yip K, Woloszyn M, Zheng MH, Tan RX (2009) NF-kappaB modulators in osteolytic bone diseases. Cytokine Growth Factor Rev 20:7–17. https://doi.org/10.1016/j.cytogfr.2008.11.007

Yang B, Li S, Chen Z, Feng F, He L, Liu B, He T, Wang X, Chen R, Chen Z, Xie P, Rong L (2020) Amyloid β peptide promotes bone formation by regulating Wnt/β-catenin signaling and the OPG/RANKL/RANK system. Faseb j 34:3583–3593. https://doi.org/10.1096/fj.201901550R

Yasuda H (2021) Discovery of the RANKL/RANK/OPG system. J Bone Miner Metab 39:2–11. https://doi.org/10.1007/s00774-020-01175-1

Yasuda H, Shima N, Nakagawa N, Mochizuki SI, Yano K, Fujise N, Sato Y, Goto M, Yamaguchi K, Kuriyama M, Kanno T, Murakami A, Tsuda E, Morinaga T, Higashio K (1998) Identity of osteoclastogenesis inhibitory factor (OCIF) and osteoprotegerin (OPG): a mechanism by which OPG/OCIF inhibits osteoclastogenesis in vitro. Endocrinology 139:1329–1337. https://doi.org/10.1210/endo.139.3.5837

Zhang Q, Tang X, Liu Z, Song X, Peng D, Zhu W, Ouyang Z, Wang W (2018) Hesperetin prevents bone resorption by inhibiting RANKL-induced osteoclastogenesis and Jnk mediated Irf-3/c-Jun activation. Front Pharmacol 9:1028. https://doi.org/10.3389/fphar.2018.01028

Zhao Y, Wang HL, Li TT, Yang F, Tzeng CM (2020) Baicalin ameliorates dexamethasone-induced osteoporosis by regulation of the RANK/RANKL/OPG signaling pathway. Drug Des Devel Ther 14:195–206. https://doi.org/10.2147/dddt.S225516